Acta Mechanica 123, 75–87 (1997)

ACTA MECHANICA

A non-Darcy model for recirculating flow through a fluid-sediment interface in a cylindrical container

A. Khalili, Bremen, Germany, **A. J. Basu,** Bangalore, India, and **M. Huettel,** Bremen, Germany

(Received May 8, 1996)

Summary. A numerical investigation has been undertaken to characterize the axisymmetric laminar flow generated by a rotating disk inside a cylinder with an open top, containing a viscous fluid above as layer of fluid-saturated porous medium. The mathematical model is based on a continuum approach for both fluid and porous regions. Attention is focussed on conditions favouring steady, stable, axisymmetric solutions of the Darcy-Brinkman-Lapwood equation. The accuracy of the method is verified by solving some vortex flow problems in disk-cylinder geometries and comparing the results with: (*a*) existing numerical solutions and, (*b*) experimental pressure measurements in a similar geometry. Calculations are performed to investigate the fluid exchange between the porous region (porewater) and the overlying water. Results indicate that flow through composite (fluid-sediment) systems can be handled with good accuracy by the method presented here. With our approach the magnitude of advective porewater transport in sediments may be predicted. This finding is important for improved designs of flux chambers and also for understanding advective transport phenomena.

Notation

B	binary parameter (0 or 1)
Da	Darcy number
K	permeability of the porous medium
H	Height
L	reference length
p	pressure
R	radius
Re	Reynolds number
t	time
u	radial velocity component
U	reference velocity
v	azimuthal velocity component
v	seepage velocity
V	intrinsic velocity
w	axial velocity component

Greek symbols

ε	porosity (fluid volume/total volume)
η	azimuthal component of vorticity
μ	dynamic viscosity
$\tilde{\mu}$	effective viscosity
Ω	angular velocity
ψ	streamfunction
ϱ	fluid density

Subscripts

d	disk
i, j	coordinates of the grid points in $r - z$ plane
p	porous medium
dp	disk to porous medium

Superscipts

*	non-dimensional parameters

1 Introduction

Study of mass and heat transfer in porous sediments on one hand, and through water-sediment interfaces on the other, has become essential for the understanding of biological processes and geochemical cycles of elements in aquatic systems. Sedimentation [1], diffusion [2], bioturbation [3] and advective interfacial flows [4] are examples of such transfer processes which link the water column production to the sedimentary degradation processes: energy-rich organic matter is incorporated into the sea bed where it is decomposed with electron acceptors (e.g. O_2, NO_3^-, SO_4^-) originating from the water column while nutrients and CO_2, the products of remineralization, are released from the sediment [5]. Likewise, pollutants adsorbed to sedimenting particles are buried and may re-enter the food chain when the geochemical environment causes desorption, thus increasing their mobility (see for example [6]).

So far, the conventional approach to study these geochemical and biological phenomena has been to collect a sediment sample from the sea-bed, bring it up to the surface and then make observations and carry out experiments on it either on-board ship or in the laboratory. Methods that have been used to evaluate biogeochemical activities in sediments and at the water-sediment interfaces are mostly experimental (except for a few numerical works which account for the convective transport, (e.g., Savant et al. [4], Svenson and Rahm [7], Svenson and Rahm [8]) and include direct measurements of benthic fluxes during the incubations of sediment together with the overlying water, and measurements of solute distributions in and above sediments (Malan and McLachlan [9]).

In the last deacade, in-situ measurements or direct experiments at the sea-bed were preferably carried out in so-called benthic landers to assure a better reproduction of the real biogeochemical processes in the samples rather than bringing them up to the surface which would subject them to large pressure and temperature gradients (Tengberg et al. [10]).

The purpose of this paper is to report the results of a numerical-theoretical study of the fluid exchange processes in composite systems (fluid overlying a fluid-saturated porous sediment). The primary aim is to examine to what extend the fluid flow in composite systems (here, in centrally stirred chambers) can be reproduced by a mathematical approach. In this paper, the emphasis is put on the hydrodynamical quantities involved, such as the velocity components and the pressure. This will form the basis for our future investigations concerning the question of how far the exchange of nutrients, toxins and solutes can be considered to be the result of non-diffusional but convective processes.

The geometrical configuration considered here (Fig. 1) consists of a circular rotating disk inside a stationary cylinder with two different regions: region *I* filled with a viscous medium only (in this case, water) with the disk rotating in it, and region *II*, the lower part of the cylinder,

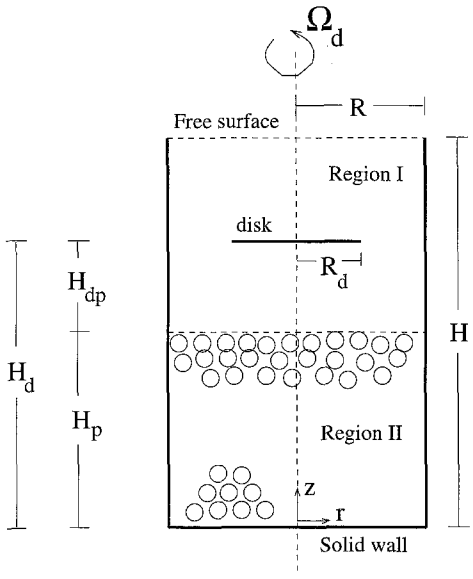

Fig. 1. Geometry of the system

containing a fluid-saturated porous sediment. The reasons for this choice are two-fold. First, it allows a better comparison of our results with the experimental investigations of Huettel and Gust [11]. Second, this geometry is frequently used in benthic landers to maintain well-known and stable hydrodynamical conditions [10]. The flow structure of the present geometry may be described as follows: in the fluid layer, we have a fully three-dimensional motion. A primary motion perpendicular to $r - z$ plane (due to the rotation of the disk) and a secondary motion in the $r - z$ plane (because of the combined effect of the rotating disk along with the existence of the stationary side walls). However, the flow is primarily two-dimensional in the porous layer as we will demonstrate in the next sections. For the numerical simulations presented here we assume axisymmetry. This assumption is justified by the well-known axisymmetric flow structure in disk-cylinder geometries for moderate Reynolds numbers as shown by Escudier [12]. In the present paper we examine the behaviour of the secondary motion which causes the percolation of fluid through the porous region and thus the exchange of fluid between the pore water and the overlying water.

The numerical study presented here is based on a continuum approach for both the fluid and the porous layer. The governing equations of motion are formulated in a general way and contain a binary parameter. Depending on the value of this parameter, the Navier-Stokes equation (Batchelor [13]) in the fluid layer and the Darcy-Brinkman-Lapwood equation in the porous layer (Lapwood [14], Wooding [15] and Nield and Bejan [16]) can be derived. However, the equation of continuity of fluid flow remains the same in both regions. The Darcy-Brinkman-Lapwood formulation combined with the continuum approach provides two advantages: first it accounts for both, the nonlinear and viscous drag which are neglegted in the original Darcy equation (compare with Batchelor [13], Dullien [17] and Scheidegger [18]) second, the continuum approach does not require any conditions for the hydrodynamical quantities at the interface and as a consequence, the numerical simulation remains independent of any additional material-dependent parameters which are usually needed when the Beavers and Joseph condition [19] is applied.

In the next section, the mathematical formulation and the detail of the numerical method used, are described.

2 Assumptions and mathematical fomulations

2.1 Assumptions

The geometrical configuration for the problem investigated here is shown in Fig. 1. As shown in the figure, a cylinder of height H and radius R, filled with water (free surface at the top) contains in its lower part a fluid-saturated porous sediment of depth H_p. The circular disk of radius R_d is positioned at a distance H_{dp} above the sediment surface and rotates about the z-axis with a uniform angular velocity Ω_d. The fluid is assumed to be incompressible and Newtonian. The porous matrix is considered to be homogeneous and having uniform permeability and porosity both not varying with time. The free surface of the fluid is assumed to remain horizontal at all times.

2.2 Mathematical formulations

with the above-mentioned assumptions, the governing equation (in vector notation) for the fluid flow in both regions I and II may be written as:

$$\varrho\left[\frac{\partial \boldsymbol{V}}{\partial t}+(\boldsymbol{V}\cdot\nabla)\,\boldsymbol{V}\right]=-\nabla p-B\left(\frac{\mu}{K}\boldsymbol{v}\right)+\tilde{\mu}\nabla^2\boldsymbol{v} \tag{1}$$

where B is a binary parameter and takes the values *zero* in the fluid layer and *one* in the porous layer. We get, in the former case, the Navier-Stokes equation for the fluid region and in the latter, the Darcy-Brinkman-Lapwood equation (see for example [20], [21] and [22]) for the fluid flow in the porous layer.

Equation (1), for both choices of the binary parameter B, has to be solved using the appropriate initial and boundary conditions in agreement with the equation of continuity, which, for a constant property fluid takes the form

$$\nabla\cdot\boldsymbol{v}=0 \tag{2}$$

in both regions.

In Eq. (1)–(2), K denotes the permeability of the porous medium and is assumed to be a scalar because of the isotropic nature of the porous medium considered here; $\tilde{\mu}$ represents the effective viscosity which is taken to be the same as μ (dynamic viscosity) in both regions, for simplicity and as suggested by Brinkman [21]. Further, p, ϱ and t are the fluid pressure, density and time, respectively. The average of the fluid velocity over an elementary volume (of solid matrix plus fluid) is called the seepage velocity and is denoted by $\boldsymbol{v}$, while the average of the same quantity over the fluid volume only, is called intrinsic velocity and denoted by $\boldsymbol{V}$. The symbol ∇ is the usual gradient operator which has to be written in the cylindrical coordinates for the purpose of this paper.

The quantities $\boldsymbol{v}$ and $\boldsymbol{V}$ are related to each other by the Dupuit-Forchheimer relationship [16]

$$\boldsymbol{v}=\varepsilon\boldsymbol{V}, \tag{3}$$

with ε denoting the porosity. Therefore, in region I, where $\varepsilon=1$, the quantities $\boldsymbol{V}$ and $\boldsymbol{v}$ are the same.

Introducing the reference length L and reference velocity U to define non-dimensional variables (denoted by *)

$$v^* = \frac{v}{U}, \quad V^* = \frac{V}{U}, \quad p^* = \frac{p}{\rho U^2}, \quad t^* = \frac{t}{(L/U)}, \quad \nabla^* = \nabla L \tag{4}$$

and replacing V by v using the Dupuit-Forchheimer relationship (and dropping the *), Eq. (1) may be written in the following dimensionless form

$$\frac{1}{\varepsilon}\frac{\partial v}{\partial t} + \frac{1}{\varepsilon^2}(v \cdot \nabla)\, v = -\nabla p - \frac{B}{\mathrm{DaRe}}\, v + \frac{1}{\mathrm{Re}}\nabla^2 v, \tag{5}$$

whereas Eq. (2) remains unchanged. Here, Re and Da are Reynolds and Darcy number, respectively, defined[1] as $\mathrm{Re} = \rho LU/\mu$ and $\mathrm{Da} = K/L^2$. Because of the geometry used in this paper, a cylindrical coordinate system (r, θ, z) is introduced, and Eqs. (2)–(5) are written for the r (radial), θ (azimuthal) and z (axial) directions (see Appendix).

Further, the equation of continuity (2) is used to introduce a streamfunction ψ, defined by

$$u = -\frac{1}{r}\frac{\partial \psi}{\partial z}, \tag{6}$$

$$w = +\frac{1}{r}\frac{\partial \psi}{\partial r}, \tag{7}$$

and the pressure is eliminated from Eq. A1–A3 (see Appendix), resulting in the following equations

$$\frac{1}{\varepsilon}\frac{\partial \eta}{\partial t} + \frac{1}{\varepsilon^2}\left(u\frac{\partial \eta}{\partial r} + w\frac{\partial \eta}{\partial z} - \frac{u}{r}\eta - \frac{2v}{r}\frac{\partial v}{\partial z}\right) = -\frac{B}{\mathrm{DaRe}}\eta + \frac{1}{\mathrm{Re}}\left(\frac{\partial^2 \eta}{\partial r^2} + \frac{1}{r}\frac{\partial \eta}{\partial r} - \frac{\eta}{r^2} + \frac{\partial^2 \eta}{\partial z^2}\right), \tag{8}$$

$$\frac{1}{\varepsilon}\frac{\partial v}{\partial t} + \frac{1}{\varepsilon^2}\left(u\frac{\partial v}{\partial r} + w\frac{\partial v}{\partial z} + \frac{u}{r}v\right) = -\frac{B}{\mathrm{DaRe}}v + \frac{1}{\mathrm{Re}}\left(\frac{\partial^2 v}{\partial r^2} + \frac{\partial^2 v}{\partial z^2} + \frac{1}{r}\frac{\partial v}{\partial r} - \frac{v}{r^2}\right), \tag{9}$$

for the entire domain taking into account different values for B. The azimuthal component of vorticity η is defined as

$$\eta = \frac{\partial u}{\partial z} - \frac{\partial w}{\partial r},$$

so that

$$-r\eta = \frac{\partial^2 \psi}{\partial r^2} + \frac{\partial^2 \psi}{\partial z^2} - \frac{1}{r}\frac{\partial \psi}{\partial r}. \tag{10}$$

The pressure in the entire domain is obtained by taking the divergence of Eq. (1) and using the continuity equation (2). The resulting equation is called the Poisson equation for pressure and may be written in vector form and discretized in time as

$$\nabla^2 p^{n+1} = -\nabla \cdot H^n, \tag{11}$$

where

$$H^n = (v^n \cdot \nabla)\, v^n. \tag{12}$$

[1] Taking the radius R_d of the disk as the characteristic length and $R_d\Omega_d$ as the reference velocity, the Reynolds and Darcy numbers for this flow can be written as $\mathrm{Re} = \rho\Omega_d R_d^2/\mu$, and $\mathrm{Da} = K/R_d^2$.

with superscripts denoting time-steps. The corresponding final equation for pressure in cylindrical coordinates is given by

$$\frac{\partial^2 p}{\partial r^2}+\frac{\partial^2 p}{\partial z^2}+\frac{1}{r}\frac{\partial p}{\partial r}=-\left(\frac{\partial u}{\partial r}\right)^2-\left(\frac{\partial w}{\partial z}\right)^2-2\frac{\partial u}{\partial z}\frac{\partial w}{\partial r}+\frac{2v}{r}\frac{\partial v}{\partial r}-\frac{u^2}{r^2}. \tag{13}$$

2.3 Initial and boundary conditions

To solve the Eqs. (8)–(10), proper initial and boundary conditions are required. In order to verify and compare our results with those obtained in the existing literature and also to give more insight into the physics of the problem, we consider here two different cases. The first case, where the fluid fills the entire container and, the second, where there is a layer of fluid-saturated porous medium at the bottom of the fluid-filled container.

2.3.1 Initial conditions

The disk, the rigid endwalls and the fluid are stationary for $t \leqq 0$. The disk is set into a constant rotation for $t > 0$. Thus the initial conditions may be written as

$\psi, v, \eta = 0$ at $t \leqq 0$ and for all r and z

$v = r\Omega_d$ at $t > 0$ and for $0 < r < R_d$, $z = H_d$

Note that conditions for η and ψ are all derived from equations for u and w.

2.3.2 Boundary conditions for ψ, v and η

For both cases the fluid-filled and fluid-sediment filled cylinder, we apply no-slip conditions at all rigid walls, free surface cndition at the top surface and symmetry condition at the axis to get

$$\psi = 0, \quad v = 0, \quad \eta = 0 \qquad \text{at} \quad r = 0, \quad < z < H$$

$$\psi = 0, \quad v = 0, \quad \eta = -\frac{1}{r}\frac{\partial^2 \psi}{\partial r^2} \qquad \text{at} \quad r = R, \quad 0 < \ < H$$

$$\psi = 0, \quad v = 0, \quad \eta = -\frac{1}{r}\frac{\partial^2 \psi}{\partial z^2} \qquad \text{at} \quad 0 \leqq r \leqq R, \quad z = 0$$

$$\psi = 0, \quad \frac{\partial v}{\partial z} = 0, \quad \eta = 0 \qquad \text{at} \quad 0 \leqq r \leqq R, \quad z = H$$

$$\psi = 0, \quad v = r\Omega_d, \quad \eta = -\frac{1}{r}\frac{\partial^2 \psi}{\partial z^2} \qquad \text{at} \quad 0 \leqq r \leqq R_d, \quad z = H_d$$

It should be emphasized that the vorticity distribution at the top side of the rotating disk differs from that at the bottom, a fact which is taken care of during the actual finite-difference formulation described in the next section.

2.3.3 Boundary conditions for p

The boundary conditions for pressure at the solid walls are derived from the governing equation of motion along the direction perpendicular to each wall. At the symmetry axis, the normal gradient of pressure is taken to be *zero*. At the free surface on top, the pressure is assumed to be

constant (ambient pressure) and is taken to be *one*. The precise form of the boundary conditions are given below:

$$\frac{\partial p}{\partial r} = 0 \qquad \text{at} \quad r = 0, \quad 0 < z < H$$

$$\frac{\partial p}{\partial r} = \frac{1}{\mathrm{Re}}\left(\frac{\partial^2 u}{\partial r^2} + \frac{1}{r}\frac{\partial u}{\partial r}\right) \qquad \text{at} \quad r = R, \quad 0 < z < H$$

$$\frac{\partial p}{\partial z} = \frac{1}{\mathrm{Re}}\frac{\partial^2 w}{\partial z^2} \qquad \text{at} \quad 0 \leqq r \leqq R, \quad z = 0$$

$$p = 1 \qquad \text{at} \quad 0 \leqq r \leqq R, \quad z = H$$

$$\frac{\partial p}{\partial z} = \frac{1}{\mathrm{Re}}\frac{\partial^2 w}{\partial z^2} \qquad \text{at} \quad 0 \leqq r \leqq R_d, \quad z = H_d$$

2.4 The finite-difference formulation

To solve the differential equations of motion a combination of various numerical techniques is used. First, we make use of the Arakawa scheme [23] to discretize the advective terms in the governing equation (1). Arakawa showed that the advective part can be written in terms of a Jacobian J, for example, as $J(\psi, v) = \partial\psi/\partial r\ \partial v/\partial z - \partial\psi/\partial z\ \partial v/\partial r$. This Jacobian can then be cast in a special finite-difference form that conserves energy. The resulting numerical scheme is fourth-order accurate in space. Next, a second-order accurate central-difference formulation is applied to discretize the viscous terms. The Poisson equations for streamfunction and pressure (10) and (13) are also solved using second-order accurate schemes. The iterations were performed using the Successive Over-Relaxation (SOR) scheme [24].

The time-integration is done by a second-order accurate explicit Adams-Bashforth scheme [25] which can be written as

$$v^{n+1} = v^n + \frac{\Delta t}{2}(3F^n - F^{n-1})$$

where the superscripts refer to the time-steps, Δt is the non-dimensional time-step and F^n refers to the time-derivative $\partial v/\partial t$ at the n-th time-step.

In the following, a brief description of some further details of the numerical scheme applied are given. In all computations uniform grids were used. The rotating disk is assumed to be infinitesimally thin so that the interface between the water and the porous layer falls at some horizontal grid-line. The streamfunction ψ and the azimuthal velocity v are equal at the top and the bottom surfaces of the rotating disk, as can be verified from the boundary conditions given above. However, for the vorticity and the pressure, this statement is not true and special treatment of the boundary conditions for these variables is required for top and the bottom surfaces of the disk.

For boundary conditions, second-order accurate expressions are derived using one-sided differencing except for vorticity boundary conditions which are treated to first order accuracy for reasons of stability. The boundary conditions at the top side of the disk are computed using one-sided differences using values above the disk only. Similarly, for the boundary conditions at the bottom side of the disk, only the values from below the disk are used.

3 Results and discussion

In this section, following the description of the features of the laminar flow, the results for the cases studied are presented.

The fluid, filling completely the cylindrical container, is initially ($t \leqq 0$) at rest. At time $t > 0$, the disk is impulsively set to rotate at a constant angular velocity. An Ekman boundary layer develops on the rotating disk. This rotating boundary layer acts now as a centrifugal fan, throwing fluid radially outwards in a spiralling motion and 'sucking' fluid into it from above and below. Two secondary meridional circulation regimes (one anti-clockwise recirculating zone above the disk and one clockwise below it) are then formed due to the existence of the solid walls and the rotating disk. Above the disk, the fluid which is pumped out of the Ekman layer spirals up the cylindrical wall, establishing a Stewartson layer until it reaches the top free surface (no penetration through the free surface is possible) where it is turned and advected towards the central axis. From here, the fluid then spirals down and is pumped back into the Ekman layer. The fluid below the disk spirals down the stationary sidewall, partially percolates the sediment from the vicinity of the sidewall and reaches a certain depth before it is sucked back towards the rotating disk.

We have calculated the fluid flow for different Reynolds numbers ranging from moderate to high, starting from Re = 1000 up to Re = 9948. The numerical study of this flow suggests that for high Reynolds numbers (i.e. Re = 9948, which coincides with one of the cases studied experimentally by Huettel and Gust [11]), the flow undergoes a series of transitions showing oscillatory flow patterns and does not give a clear indication of the nature of the unsteadiness. Thus, in drawing conclusions from the results, we restrict ourselves to those cases in which the assumption of axisymmetry holds and, therefore, present the flow simulation for Re = 1000 only. However, for the range of other characteristic parameters concerning the geometry and the properties of the porous medium, same values as in the experimental set-up of [11] are taken. This leads to the following normalized (with respect to $R_d = 10$ cm), dimensionless magnitudes: $R = 1.25, H = 3, R_d = 1, H_d = 2.5, \Omega_d = 1, H_p = 1.5, H_{dp} = 1.0, \varepsilon = 0.346$. Taking the permeability to be $K = 1.4805 \times 10^{-11}$ m^2, we obtain a Darcy number of Da $= 1.4805 \times 10^{-9}$.

Uniform grids of 51×121 and 101×241 mesh points were used to simulate flow fields at Reynolds numbers of 1000 and 9948, respectively. The stability of the computation was ensured by taking a time-step[2] $\Delta t = 0.0005$ for fluid-filled and $\Delta t = 0.000004$ for water-sediment filled container.

The accuracy of the numerical results of the method presented here is verified by reproducing the experimental visualizations of Escudier [12] and numerical results of Lopez [26] for the flow of a viscous fluid in a cylindrical container at rest with a rotating lid, and by comparing our results for the fluid-filled container with the results obtained by Khalili et al. [27]. In both cases, the agreement is found to be very good. Further, the results of the pressure calculation for the fluid-porous filled cylinder are compared with the experimental measurements of Huettel and Gust [11] which will be shown below.

As the flow is axisymmetric, the attention for the numerical integration (Fig. 2 to Fig. 5) is confined to the right half of the container (Fig. 1) and the flow field is shown in this area only.

Figure 2 shows the development of the streamfunction contours, i.e. intersection of stream surfaces ψ with the meridional plane for the fluid-filled cavity from an early stage (Fig. 2a) upto the steady state (Fig. 2f). The maximum change anywhere in the flow-field over a time-step was

[2] In non-dimensional time-units.

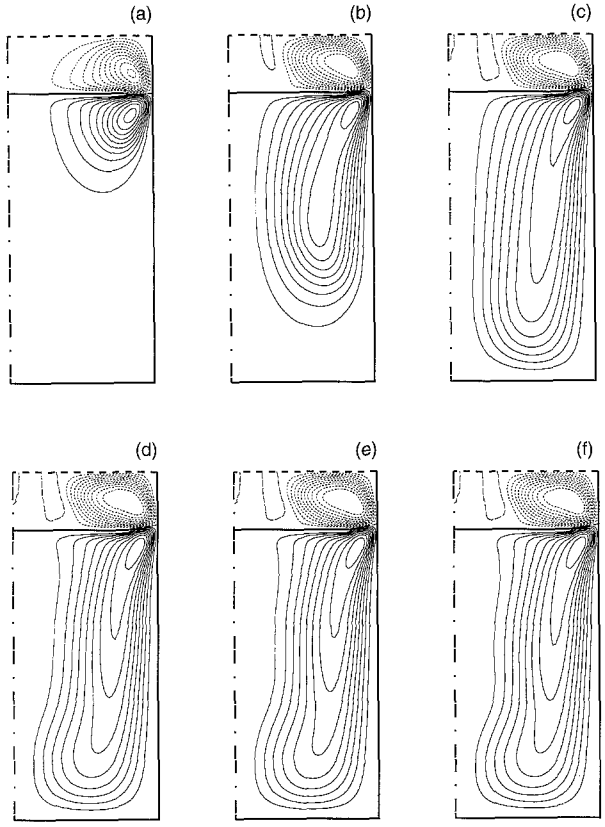

Fig. 2. Temporal development of streamlines for the fluid-filled container (Re = 1000) **a** $t = 10$, **b** $t = 50$, **c** $t = 100$, **d** $t = 150$, **e** $t = 200$, **f** $t = 242$

calculated for all variables at each time-step and time-integration was terminated when the conditions $\psi_{i,j}^{n+1} - \psi_{i,j}^{n} \leqq 10^{-9}$, $v_{i,j}^{n+1} - v_{i,j}^{n} \leqq 10^{-8}$, and $\eta_{i,j}^{n+1} - \eta_{i,j}^{n} \leqq 10^{-7}$ were achieved at all mesh points. Note that the dotted lines denote an anti-clockwise rotation whereas the solid ones indicate a clockwise rotation. As can be seen from these figures, the distribution of the secondary motion, though initially restricted in the vicinity of the rotating disk, occupies the entire domain with increasing time.

Figure 3 compares the steady state contours of the streamfunction ψ of both cases, that of the fluid-filled container (Fig. 3 a) with the fluid-sediment filled container (Fig. 3 b, sediment layer shown in grey). Because of high resistance to the flow by the sediment layer, the secondary flow penetrates the porous medium only to a certain depth, leaving a considerable part of the underlying pore-water region at rest. For a better comparison of the flow in the two cases, we have depicted the $\psi = 0.002$ streamlines as a dashed-dotted line. As can be seen from the figures, this relatively weak flow nearly reaches the bottom of the cylinder in the first case (Fig. 3 a) whereas it is damped in the sediment layer (Fig. 3 b).

When the cylinder contains porous material, we observed that the steady state is reached in a shorter time ($t = 100$) compared with a pure fluid-filled container ($t = 242$). This is due to the stabilizing effect of friction imposed on the fluid particles.

The distribution of η, the azimuthal component of the vorticity vector, is shown in Fig. 4. As can be seen, the strong vortex sheet is mainly confined to a region in the vicinity of the rotating disk with relatively small vorticity away from it in the case of the fluid-filled cavity (Fig. 4 a). In contrast, the vorticity in the porous region (Fig. 4 b) is nearly zero, as in this region the azimuthal gradient of the radial velocity components balance the radial gradients of the axial velocity, resulting in a quasi-irrotational flow there.

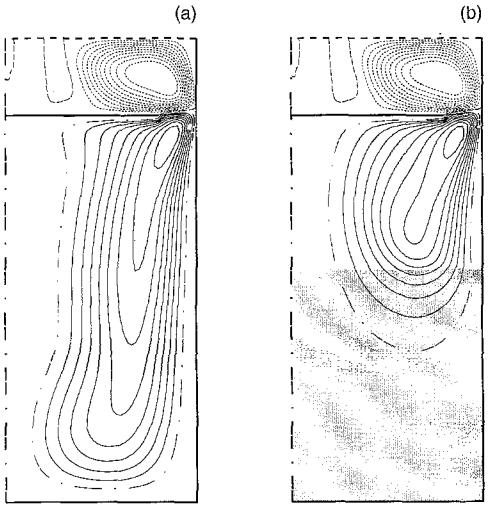

Fig. 3. Comparison of the steady-state streamlines for Re = 1000 (min. = −0.02, max. = +0.02, $\Delta\psi = 0.002$), dashed-dotted line $\psi = 0.002$. **a** Fluid-filled container, **b** fluid and sediment-filled (grey region) container

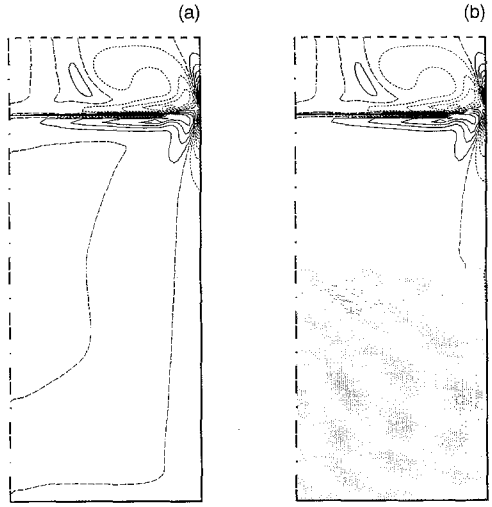

Fig. 4. Lines of constant azimuthal vorticity η for Re = 1000 (min. = −10, max. = +10, $\Delta\eta = 1$). **a** Fluid-filled container, **b** fluid and sediment-filled (grey region) container

The computed results for the tangential velocity component v are shown in Fig. 5 a and 5 b. In the absence of the porous layer, the entire fluid body is set into rotation in θ direction (with decreasing velocity away from the disk) and in circulation in the $r - z$ plane, whereas it remains free of tangential velocity in the porous region. Thus the flow in the porous layer is primarily two-dimensional and takes place in the $r - z$ plane only. Also in the graph (Fig. 5) showing the distribution of the tangential velocity component v, a dashed-dotted line for $v = 0.05$ is depicted to demonstrate the different positions of the equivalent contours.

Of particular interest is the distribution of the computed differential pressure at the water-sediment interface along the container radius from the central axis towards the vertical outer wall. As can be seen from Fig. 6, the pressure initially increases, reaches a point of inflection and, at the outer wall, then has almost zero radial gradient. Though the Reynolds number corresponding to this picture is 1000, the qualitative behaviour is the same as that of the experimental measurements of [11] and Glud et al. [28].

The calculations shown above stress the importance of secondary flows and related advective porewater exchange for flux measurements in benthic chambers deployed on permeable sea beds. As illustrated by the streamline contours (Fig. 4) the ensuing porewater flows flush the upper layers of the sediment to a certain depth defined by the permeability K of the incubated core and

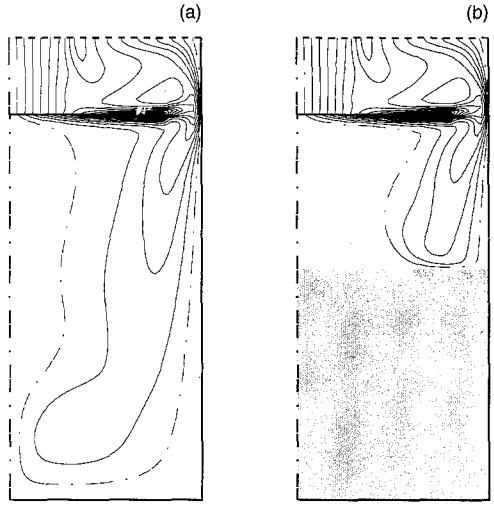

Fig. 5. Lines of constant tangential velocity v for Re = 1000 (min. = 0, max. = 1, $\Delta v = 0.05$), dashed-dotted line $v = 0.05$. **a** Fluid-filled container, **b** fluid and sediment-filled (grey region) container

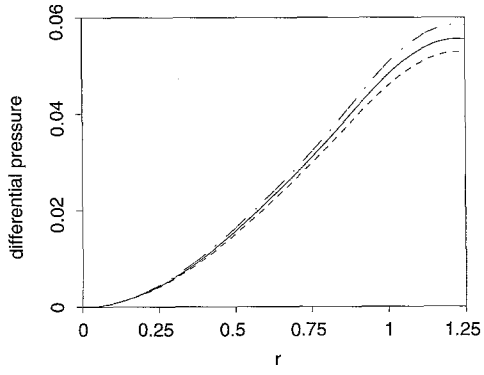

Fig. 6. Radial distribution of differential pressure at the fluid-sediment interface. Dashed, continuous and dashed-dotted lines denote a grid point below, at and above the interface respectively

the magnitude of the secondary flow. Calibration experiments performed by Glud et al. [29] with two common benthic chamber designs with central stirring of different angular velocities indicate advective porewater flushing in natural sediments with $K > 10^{-12}$ m^2. Also Huettel and Gust [11] observed similar phenomena in water-sediment filled containers with stirring devices and concluded that advective flushing can enhance interfacial solute flux up to 6-fold (with chamber water reaching 8-fold deeper into the sediment) compared to reference sediments exposed to two-dimensional flow in a straight open channel. Since most of the highly degradable sedimented organic matter is concentrated in the upper centimeter of the sea bed (Berner [5]), the stirring induced directed porewater exchange affects the most sensitive geochemical reaction zone. The model presented here allows us to define the precise conditions (depending on the physical property of the sediment, position, size and angular velocity of the rotating disk) under which flux measurements can be performed unaffected by advective porewater flushing.

4 Conclusions

A numerical solution of the axisymmetric Darcy-Brinkmann-Lapwood equation has been obtained and used to examine the fluid exchange in a composite fluid-sediment layer. The accuracy of the numerical solutions has been established by: (a) comparing them with well

known solutions of fluid flow in disk-cylinder geometries, (b) qualitative comparison with available experimental results and, (c) varying the grid resolution. The qualitative agreement between the numerical solutions and the experimental measurements and visualizations is found to be good. Certain quantities of the flow particularly interesting for interfacial solute fluxes in marine environments, such as the penetration depth of the flow into a permeable sediment can be obtained by the approach detailed in this paper and a clear picture of the topology of the flow can be shown, which is not easy by experimental visualizations or measurements. A number of interesting questions remain. Is it possible to simulate the same flow assuming a potential flow in the porous layer? Is Darcy's law applicable in the case of a multidirectional flow, where the flow has a component perpendicular to the fluid-porous interface? To investigate these questions is our future aim.

Appendix

Equations of motion in cylindrical coordinate system (axisymmetric)

$$\frac{1}{\varepsilon}\frac{\partial u}{\partial t}+\frac{1}{\varepsilon^2}\left(u\frac{\partial u}{\partial r}+w\frac{\partial u}{\partial z}-\frac{v^2}{r}\right)=-\frac{\partial p}{\partial r}-\frac{B}{\mathrm{DaRe}}u+\frac{1}{\mathrm{Re}}\left(\frac{\partial^2 u}{\partial r^2}+\frac{1}{r}\frac{\partial u}{\partial r}-\frac{u}{r^2}+\frac{\partial^2 u}{\partial z^2}\right) \tag{A.1}$$

$$\frac{1}{\varepsilon}\frac{\partial v}{\partial t}+\frac{1}{\varepsilon^2}\left(u\frac{\partial v}{\partial r}+w\frac{\partial v}{\partial z}+\frac{uv}{r}\right)=-\frac{B}{\mathrm{DaRe}}v+\frac{1}{\mathrm{Re}}\left(\frac{\partial^2 v}{\partial r^2}+\frac{1}{r}\frac{\partial v}{\partial r}-\frac{v}{r^2}+\frac{\partial^2 v}{\partial z^2}\right) \tag{A.2}$$

$$\frac{1}{\varepsilon}\frac{\partial w}{\partial t}+\frac{1}{\varepsilon^2}\left(u\frac{\partial w}{\partial r}+w\frac{\partial u}{\partial z}\right)=-\frac{\partial p}{\partial z}-\frac{B}{\mathrm{DaRe}}w+\frac{1}{\mathrm{Re}}\left(\frac{\partial^2 w}{\partial r^2}+\frac{1}{r}\frac{\partial w}{\partial r}+\frac{\partial^2 w}{\partial z^2}\right) \tag{A.3}$$

By taking $\partial/\partial z$ (A.1) $-$ $\partial/\partial t$ (A.3), pressure can be eliminated from these equations and the streamfunction-vorticity formulation can be derived.

Continuity equation in cylindrical coordinate system (axisymmetric)

$$\frac{\partial u}{\partial r}+\frac{u}{r}+\frac{\partial w}{\partial z}=0. \tag{A.4}$$

Acknowledgements

We would like to thank Prof. Roddam Narasimha for many interesting discussions on this subject and Prof. B. B. Jørgensen for his support. AJB would like to thank MPI-MM, Bremen, for hospitality received. AK would like to thank JNCASR, Bangalore, for the same reason.

References

[1] Alldrege, A. L., Gotschalk, C.: In situ settling behavior of marine snow. Limnol. Oceanogr. **33,** 339–351 (1988).

[2] Jørgensen, B. B., Revsbech, N. P.: Diffusive boundary layers and the oxygen uptake of sediments detritus. Limnol. Oceanogr. **30,** 111–122 (1985).

[3] Aller, R. C.: Experimental studies of changes produced by deposit feeders on pore water, sediment, and overlying water chemistry. Am. J. Sci. **278,** 1185–1234 (1978).

[4] Savant, S. A., Reible, D. D., Thiboeaux, L. J.: Convective transport within stable river sediments. Water Resources Res. **23,** 1763–1768 (1987).
[5] Berner, R. A.: Early diagenesis: A theoretical approach. Princeton 1980.
[6] Swartz, R. C., Lee, H.: Biological process affecting the distribution of pollutants in marine sediments. Part I. Accumulation, trophic transfer, biodegradation and migration. In: Contaminants and sediments, Vol. 2, Baker, R. A., Ed., pp. 5–45. Butterworth: Ann Arbor. 1980.
[7] Svenson, U., Rahm, L.: Modelling the near-bottom region of the benthic boundary layer. J. Geophys. Res. **93,** 6906–6915 (1988).
[8] Svenson, U., Rahm, L.: Towards a mathematical model of oxygen transfer to and within bottom sediments. J. Geophys. Res. **96,** 2777–2783 (1991).
[9] Malan, D. E., McLachlan, A.: In situ benthic oxygen fluxes in a nearshore coastal marine system: a new approach to quantify the effect of wave action. Mar. Ecol. Prog. Ser. **73,** 69–81 (1991).
[10] Tengberg, A., et al.: Benthic chamber and profiling landers in oceanography: A review of design, technical solutions and functionality. Prog. Oceanogr. **35,** 253–294 (1995).
[11] Huettel, M., Gust, G.: Solute release mechanisms from confined sediment cores in stirred benthic chambers and flume flows. Mar. Ecol. Prog. Ser. **82,** 187–197 (1992).
[12] Escudier, M. P.: Observations of the flow produced in a cylindrical container by a rotating endwall. Exp. Fluids **2,** 189–196 (1984).
[13] Batchelor, G. K.: An introduction to fluid dynamics. London: Cambridge University Press, 1967.
[14] Lapwood, E. R.: Convection of a fluid in a porous medium. Proc. Camb. Phil. Soc. **44,** 508–521 (1948).
[15] Wooding, R. A.: Steady state free thermal convection of liquid in a saturated permeable medium. J. Fluid Mech. **2,** 273–285 (1957).
[16] Nield, D. A., Bejan, A.: Convection in porous media. New York: Springer 1992.
[17] Dullien, F. A. L.: Porous media: fluid transport and pore structure. New York: Academic Press (1979).
[18] Scheidegger, A. E.: The physics of flow through porous media. Toronto: University of Toronto (1974).
[19] Beavers, G. S., Joseph, D. D.: Boundary conditions at a naturally permeable wall. J. Fluid Mech. **30,** 197–207 (1967).
[20] Whitaker, S.: Flow in porous media: A theoretical derivation of Darcy's law. Trans. Porous Media **1,** 3–25 (1986).
[21] Brinkman, H. C.: A calculation of the viscous force exerted by a flowing fluid on a dence swarm of particles. Appl. Sci. Res. **A1,** 27–34 (1947).
[22] Brinkman, H. C.: On the permeability of media consisting of closely packed porous particles. Appl. Sci. Res. **A1,** 81–86 (1947).
[23] Arakawa, A.: Computational design for long-term numerical integration of the equations of fluid motion: Two-dimensional incompressible flow. Part I. J. Comput. Phys. **1,** 119–143 (1966).
[24] Peyret, R., Taylor, T. O.: Computational methods for fluid flow. New York: Springer 1983.
[25] Atkinson, K.: Elementary numerical analysis. New York: John Wiley & Sons 1985.
[26] Lopez, J. M.: Axisymmetric vortex breakdown. Part 1, Confined swirling flow. J. Fluid. Mech. **221,** 533–552 (1990).
[27] Khalili, A., Adabala, R. R., Rath, H. J.: Flow induced by an asymmetrically placed disk rotating coaxially inside a cylindrical casing. Acta Mech. **113,** 9–19 (1995).
[28] Glud, N. G., Gundersen, J. K., Revsbech, N. P., Jørgensen, B. B., Huettel, M.: Calibration and performance of the stirred flux chamber from the benthic lander ELINOR. Deap-Sea Res. **42,** 1029–1042 (1995).
[29] Glud, N. G., Forster, S., Huettel, M.: Influence of radial pressure gradients on solute exchange in stirred benthic chambers Mar. Ecol. Prog. Ser. **141,** 303–311 (1996).

Authors' addresses: A. Khalili and M. Huettel, Max-Planck-Institute for Marine Microbiology, Celsiusstr. 1, D-28359 Bremen, Germany; A. J. Basu, Jawaharlal Nehru Centre for Advanced Scientific Research, Jakkur Campus, Bangalore 560064, India